NANO LETTERS

pubs.acs.org/NanoLett Letter

AFM Unravels the Unique Adhesion Properties of the *Caulobacter* Type IVc Pilus Nanomachine

Johann Mignolet,* Albertus Viljoen, Marion Mathelié-Guinlet, Felipe Viela, Claire Valotteau, and Yves F. Dufrêne*

Cite This: *Nano Lett.* 2021, 21, 3075−3082 Read Online

ACCESS | Metrics & More | Article Recommendations | Supporting Information

ABSTRACT: Bacterial pili are proteinaceous motorized nanomachines that play various functional roles including surface adherence, bacterial motion, and virulence. The surface-contact sensor type IVc (or Tad) pilus is widely distributed in both Gram-positive and Gram-negative bacteria. In *Caulobacter crescentus*, this nanofilament, though crucial for surface colonization, has never been thoroughly investigated at the molecular level. As *Caulobacter* assembles several surface appendages at specific stages of the cell cycle, we designed a fluorescence-based screen to selectively study single piliated cells and combined it with atomic force microscopy and genetic manipulation to quantify the nanoscale adhesion of the type IVc pilus to hydrophobic substrates. We demonstrate that this nanofilament exhibits high stickiness compared to the canonical type IVa/b pili, resulting mostly from multiple hydrophobic interactions along the fiber length, and that it features nanospring mechanical properties. Our findings may be helpful to better understand the structure−function relationship of bacterial pilus nanomachines.

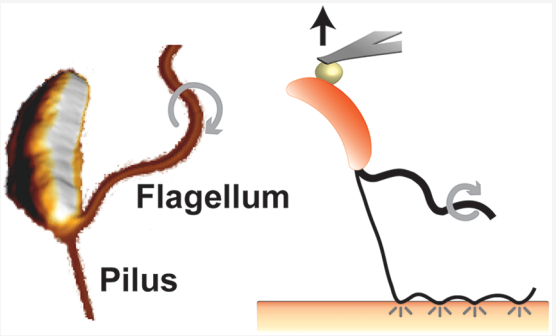

KEYWORDS: *bacterial nanomachines, type IV pili, Tad pilus, adhesion, mechanics, Caulobacter crescentus, single-cell force spectroscopy*

Bacterial cells have developed sophisticated trans-envelope nanomachines that can execute a variety of key cellular functions, such as motility, mechanosensing, substrate adhesion, and virulence.[1] Among them, type IV pili (T4P) are dynamic fibers involved in social motility, exogenous DNA acquisition, biofilm formation, and surface attachment.[2,3] They contribute to the virulence of major infectious agents, such as *Pseudomonas aeruginosa* and *Neisseria meningitidis*,[4] and are tantalizing nanostructure targets to elaborate new vaccines or antiadhesive drugs of low selective pressure.[5]

The primary role of pili is to initiate contact with surfaces and maintain it through specific and nonspecific interactions, such as receptor−ligand bonds (e.g., FimH)[6] and hydrophobic interactions in the case of the Type IVa pilus (T4aP).[7] This dampens the effects of Brownian motion and shear forces and facilitates the landing stage as pili retract. Because of their small size, these nanofilaments have long been difficult to characterize using conventional techniques. However, atomic force microscopy (AFM), pillar bending, and optical tweezers have quantified the various mechanical responses of prototypical pili. For instance, the T4aP of *Neisseria gonorrheae* sustains a tension force of ∼100 pN before it transits to a longer and thinner state.[8] The *P. aeruginosa* T4aP involved in twitching motility was reported to bind both hydrophilic and hydrophobic substrates over a significant portion of their length. They can sustain forces up to 250 pN before they break contact, which explains their resistance to mechanical stress and the broad range of surfaces that *P. aeruginosa* colonizes.[9,10] The pilins of the *Escherichia coli* type I pilus (T1P) are big β-strand proteins that adopt an immunoglobulin-like fold and assemble in a helical rod. During extension, they undergo a stepwise reversible unravelling (stacking−unstacking of pilin subunits) that generates a force plateau of about 80 pN.[11]

While T4aP and other pili have been extensively studied to evaluate their architecture and adhesiveness,[2,7] we know little about the nanobiophysics of the tight adherence (Tad) type IVc pilus (T4cP), despite their wide distribution throughout bacterial phyla.[12] Half of the ancestral Tad machinery components have no homology with known subunits of other pili or related secretion systems.[13,14] In particular, both the primary sequence and the ultrashort size of the Tad pilin (Flp), a.k.a. PilA in *Caulobacter crescentus*, strongly deviate from the T4P systems.[15] Homology modeling of the Tad pilin structure indicated that it lacks a C-terminal globular domain typical of T4a/bP and only comprises a short highly

Received: January 20, 2021
Revised: March 10, 2021
Published: March 23, 2021

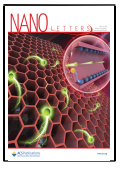

https://doi.org/10.1021/acs.nanolett.1c00215
Nano Lett. 2021, 21, 3075−3082

hydrophobic N-terminal α-helix that forms the fiber core and anchors it onto the plasma membrane.[16] Therefore, we reasoned that the fiber architecture and adhesiveness, as well as the dynamics of extension, might differ from other T4P pili.

To test this hypothesis, we used AFM[17] to unravel the nanoscale structure, adhesion and mechanics of the atypical *Caulobacter* Tad T4cP. This pilus is intricately orchestrated in space and time[13,18] and assembled solely at the flagellated cell pole of swarmer cells (Figure 1). To selectively probe the

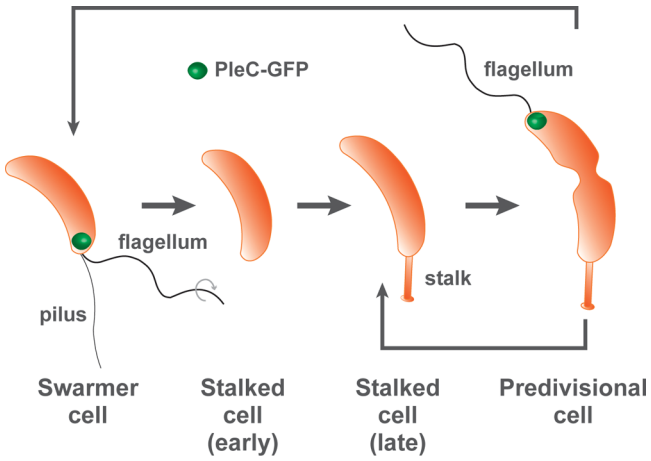

Figure 1. Tad pilus biogenesis is orchestrated during the *Caulobacter* cell cycle. Under appropriate conditions, an initial piliated and flagellated swarmer cell loses its polar appendages and differentiates into a sessile stalked cell, switching from a mobile to a sedentary and reproductive cell stage. Upon division, the mother stalked, predivisional cell yields two sibling cells with distinct cell fates, a mobile swarmer cell and a sessile stalked cell. The green ball indicates the GFP reporter fusion used in this study to discriminate between piliated and nonpiliated cell types.

adhesive properties of single Tad filaments, we implemented a novel fluorescence-based piliated cell discrimination method and combined it with AFM-based single-cell force spectroscopy (SCFS). Our data showcase the uniqueness of the Tad nanomachine adhesion and mechanics in comparison with other well-studied T4a/bP pili.

RESULTS

Nanoscale Imaging of the Slender Tad Pilus. Prior studies with epifluorescence and transmission electron microscopy (TEM) visualized the Tad pili of *Caulobacter*[19−22] and *Aggregatibacter actinomycetemcomitans*.[23] However, they required methodologies that may interfere with the pilus function, such as phages, antibody or xenobiotic labeling, and pilin mutation, and were often performed at fairly low resolution. We used AFM imaging to produce high-resolution topographic images of label-free pili (see Supporting Information Methods). To favor the piliated cell stage, we cultured *Caulobacter* in minimal medium to reach the midexponential phase ($OD^{660\ nm}$ ~0.5) and we fixed the cells with paraformaldehyde in order to prevent or dampen pilus retraction and breakage. Like *Pseudomonas aeruginosa* T4aP[9] and pili of Gram-positive bacteria,[24] Tad pili were unamenable to being imaged in liquid buffer because of their dynamics and high flexibility, and were therefore imaged in dry conditions. Deflection images showed that WT swarmer cells frequently exhibited a straight or slightly curved pilus escorted by a unique sinusoid flagellum that extruded from the same pole (Figure 2A). Most piliated cells (96%; n = 52 cells from different preparations) were decorated with a single pilus while few cells were decorated with two pili. In contrast, a hyperpiliated strain overexpressing a plasmid-borne copy of the *tad* operon ($pilus^{++}$) exhibited a greater proportion of multipiliated cells (Figure 2B). Even in flagellum-less cells, some of these cells assembled up to four pili with a structure similar to the WT. For both strains, we occasionally observed free fragments of pili, suggesting that growth conditions, sample preparation, or tip scanning may break some filaments.

Analysis of height images revealed that pili harbor a fairly constant diameter of 1.5 ± 0.4 nm, but a highly variable length, ranging from 0.4 to 4.6 μm (Figure 2C, 2D, and 2E). These values, as well as the pilus morphology, were similar in the case of a hyperpiliation phenotype, suggesting that boosting pilus gene expression modulates the number of filament assembly complexes, as previously reported,[25,26] but does not alter the intrinsic pilus structure and length. This contrasts with previous reports on Gram-positive pili and Gram-negative pseudopili (type II secretion system) that correlate pilus gene (over)expression and pilus length.[15,27] *Caulobacter* flagella have a larger diameter architecture (6.6 ± 0.6 nm) with a thicker hook section (10.9 ± 0.9 nm) and a conspicuous trans-insertion inside the diderm envelope (Figure 2A, 2B, 2C, and 2D). Taken together, these results suggest that *Caulobacter* preferentially assembles a single pilus at the flagellated pole with a diameter thinner than that of T4aP (4−6 nm).[28]

Probing the Nanoscale Adhesion between Tad Pili and Hydrophobic Substrates. While AFM- and optical tweezer-based studies have focused on T4a/bP, the adhesion and mechanics of Tad pili in live cells remain uncharacterized. We probed, under aqueous physiologically relevant conditions, the adhesive interactions between single living piliated cells and substrates exposing hydrophobic methyl groups. We used this model surface because hydrophobic interactions are one of the important driving forces for bacterial adhesion to abiotic surfaces,[29] and because the pilin subunit of the Tad pilus is highly hydrophobic. A major technical challenge is that pili are assembled only in *Caulobacter* swarmer cells, which represent a small fraction of the whole population in batch culture. To circumvent this problem, we designed a swarmer cell selection procedure relying on the PleC-GFP fluorescent fusion (Figures 1, 3A, and 3B; Supporting Information Methods). PleC is a protein morphogen that localizes at the flagellated pole in swarmer cells (smaller cell type), as well as in late predivisional cells (larger cell type).[30] We were thus able to selectively attach only single small cells with a polar fluorescent focus to the colloidal cantilevers (Figure 3B). We combined this fluorescence-based pilus screen with SCFS[31] (Supporting Information Methods) to generate force−distance (FD) curves (256 on 10 μm × 10 μm areas), thus enabling us to specifically characterize the strength and dynamics of Tad pilus adhesion. In our analyses, we considered the rupture force, corresponding to the last adhesion event just before the contact between AFM probe and substratum breaks. Markedly, the adhesion frequencies of WT piliated cells were high (Figures 3C, 4A, and 4B) with a mean percentage of 74 ± 18% (mean ± s.d., n = 2,816 curves from a total of 11 cells, Figure 4B), highlighting their high propensity to stick to hydrophobic surfaces even at small contact times (50 ms, estimated from force vs time traces). For most cells investigated, the mean rupture force was 213 ± 106 pN (mean ± s.d., n = 2,816 curves), but was

https://doi.org/10.1021/acs.nanolett.1c00215
Nano Lett. 2021, 21, 3075−3082

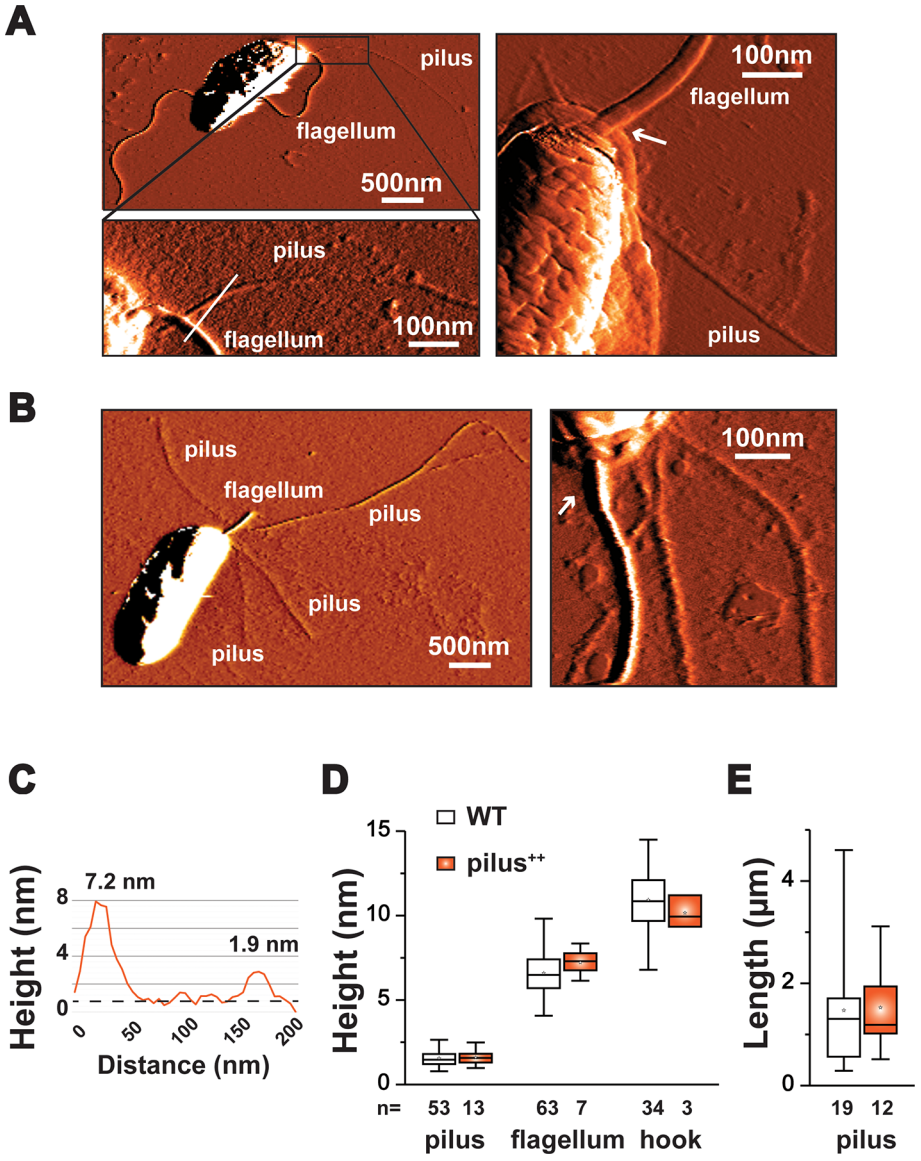

Figure 2. Nanoscale visualization of Tad filaments. (A, B) AFM deflection images of piliated and flagellated swarmer cells recorded in air for WT (A) and hyperpiliated mutant (B) strains. The white arrows in the right images pinpoint the larger shape of the flagellar hook. A zoom on the pole region (black rectangle) is shown in the bottom of panel (A). (C) Cross section taken along the white line (A, bottom) in the corresponding height image, emphasizing the pilus and flagellum diameters. (D, E) Boxplot comparison of pilus, flagellum, and flagellar hook diameters (D) and lengths (E) in WT (open bars) and hyperpiliated (pilus^{++}; orange bars) strains. The number of measurements are indicated below the bar charts (height images from 52 and 10 different cells were analyzed). Boxplots include the mean values (stars), medians (horizontal lines), 1st and 3rd quartiles (box limits), and ranges (whiskers).

occasionally as high as 458 ± 138 pN (Figures 3C, 4A, and 4C). Of note, the strength and probability of adhesion did not vary upon recording multiple consecutive curves (256 on 10 × 10 μm areas), meaning that force measurements over time did not alter the pilus properties. The hydrophobic adhesion force of T4cP is substantially larger than that of *P. aeruginosa* T4aP (around 150 pN).[9,10] We also observed high variability in rupture lengths (Figures 3C, 4A, and 4D), which may be related to the diversity of Tad filament lengths (Figure 2E).

Adhesion is abrogated in nonpiliated bacteria. Next, we asked whether the T4cP adhesive properties may be influenced by mutations or cell cycle phases that affect appendage biogenesis (flagellum or pilus). In a mutant that does not assemble a flagellar filament (Δ*fla*), piliated swarmer cells still produced frequent adhesive curves (70 ± 25%, n = 2,304 curves from a total of 9 cells) with rupture forces in the same range as that of the WT strain (182 ± 78 pN) (Figure 4A, 4B, and 4C). However, the rupture lengths, averaging at 142 ± 46 nm, were smaller than those of the WT (Figure 4D). A possible explanation is that flagellar mutations, in flagellin, hook, or motor genes, indirectly reduce the pilin steady-state level (up to 10 times) and negatively impact the pilus function. This might drive a decrease in filament length or the time window during which an assembled filament is present at the cell surface.[25]

By contrast, in a pilus-negative mutant (Δ*pilA*), the adhesion frequency was lowered to 7 ± 9% (n = 2,816 curves from a total of 11 cells) (Figure 4A and 4B), and the average force of adhesion was decreased down to 71 ± 27 pN (Figure 4A and 4C). This mutant still harbors a functional flagellum[18] but

https://doi.org/10.1021/acs.nanolett.1c00215
Nano Lett. 2021, 21, 3075−3082

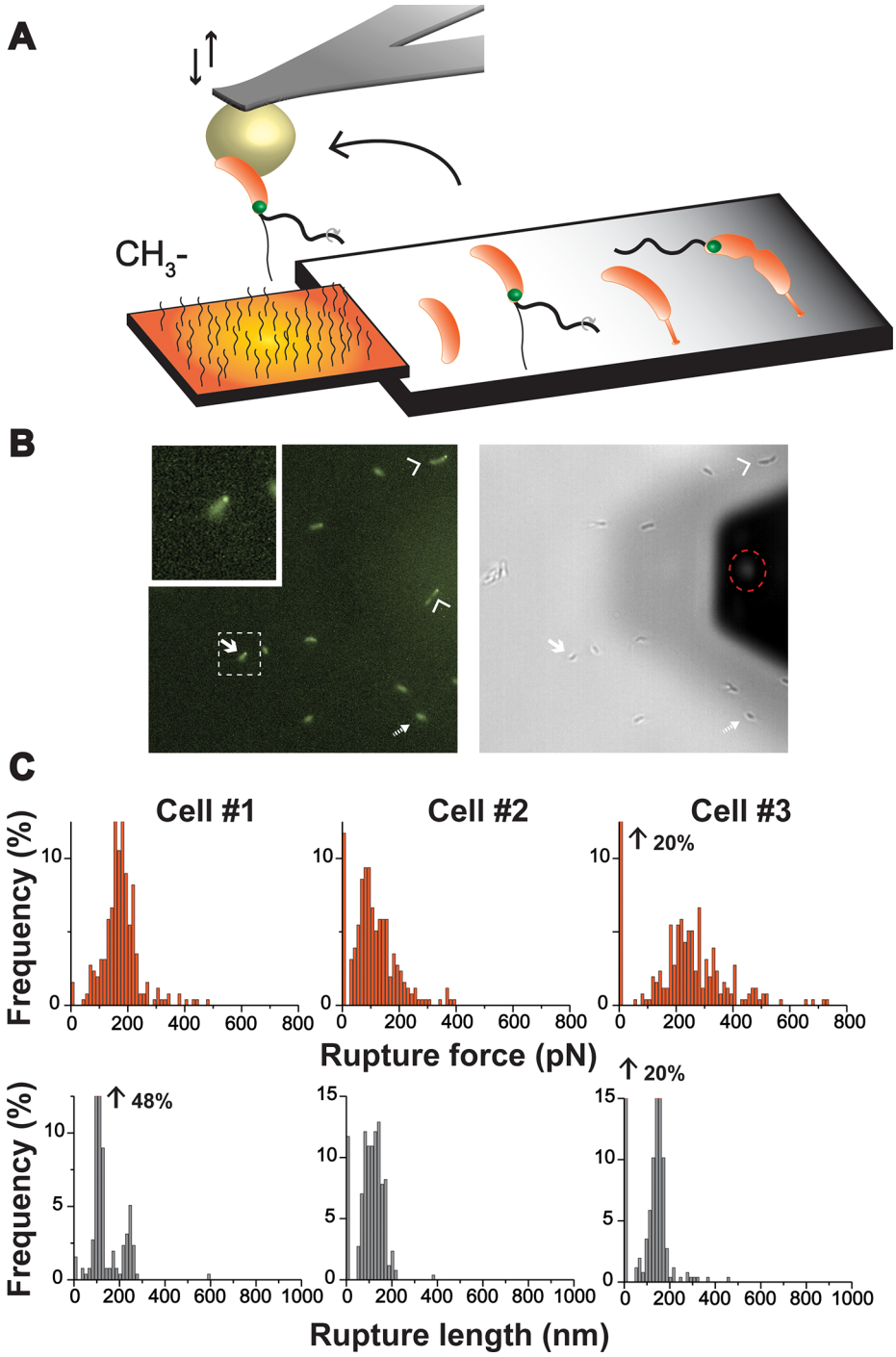

Figure 3. Quantifying the adhesion of single Tad pili in living bacteria. (A) Schematic representation depicting the cell-discrimination setup to select and probe piliated swarmer cells by single-cell force spectroscopy (SCFS). An asynchronous population of cells with fluorescence-labeled new poles (PleC-GFP) is subjected to fluorescence illumination to distinguish piliated swarmer cells (small cells; unipolar fluorescent foci) from early stalk cells (small/medium cells; no unipolar foci) or late predivisional cells (large cells; unipolar foci). The relevant cell type is transferred on a colloidal cantilever (see SI Methods) and multiple FD curves are recorded with a contact time of 50 ms, in PBS, on a hydrophobic, CH_3-terminated substrate. (B) Fluorescence and bright field optical images of WT *Caulobacter* producing a PleC-GFP fusion. During the swarmer cell discrimination procedure, small cells with a polar focus highlighted by solid arrows were considered as piliated cells (see inset in the left image for larger magnification). Small cells with no polar focus (dashed arrows) and large cells with a polar focus (arrowheads) were considered as nonpiliated cells. The red dashed circle in the right image pinpoints the colloidal bead attached to the AFM cantilever and coated with polydopamine to grab the desired cell type. (C) Representative frequency histograms of rupture forces (red), i.e. last adhesion event before detachment of the pilus, and rupture lengths (gray) for three representative WT cells probed in PBS on hydrophobic surfaces. In total, 256 curves (per cell) were recorded on 11 different cells.

exhibits a markedly reduced frequency and magnitude of hydrophobic forces, while a flagellar mutant phenocopies the WT strain. Therefore, we believe that the contribution of the flagellum in hydrophobic adhesion is minor, mainly producing

https://doi.org/10.1021/acs.nanolett.1c00215
Nano Lett. 2021, 21, 3075−3082

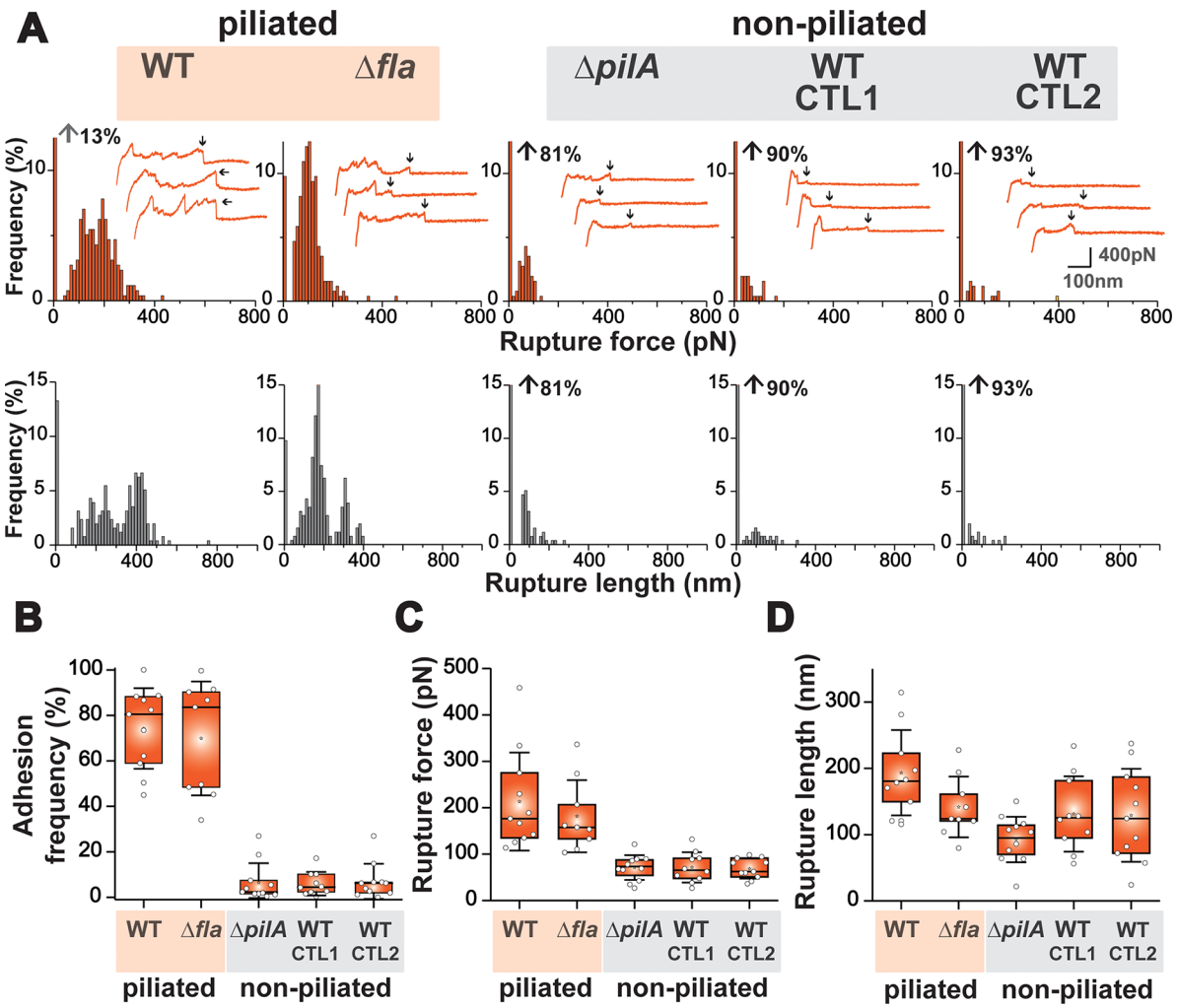

Figure 4. Piliated vs nonpiliated cell adhesion behaviors. (A) Representative frequency histograms (%) of rupture forces (red) and rupture lengths (gray) for piliated cells (WT and flagellar mutant [Δ*fla*] swarmer cells) and nonpiliated cells (pilus mutant [Δ*pilA*] swarmer cells, and WT predivisional [CTL1] or stalk [CTL2] cells). Histograms were plotted for a single representative cell for each condition (256 curves per cell were analyzed). Insets in rupture force histograms show representative retraction force curves in which rupture events are highlighted with arrows. The data are representative of a total of 11, 9, 11, 10, and 11 independent cells from the WT, Δ*fla*, Δ*pilA*, CTL1, and CTL2, respectively. (B, C, and D) Boxplots of adhesion frequencies (B), rupture forces (C), and rupture lengths (D) for the five different cell types. Boxplots include the mean values (stars), medians (horizontal lines), 1st and 3rd quartiles (box limits), standard errors (whiskers), and cells (open circles).

single defined peaks that contrast with the multicontact point adhesion of the pilus.

Our protocol also allowed us to probe hydrophobic forces at the different cell stages of WT cells that are transiently not decorated with pili. These cells consisted of two populations: big, predivisional cells with a fluorescent focus (CTL 1) and small, early stalked cells without a fluorescent focus (CTL 2) (Figures 1 and 3A). In both cell types (n = 2,560 and 2,816 curves from 10 and 11 cells, respectively), hydrophobic interactions were nearly abrogated with a sharp decrease in adhesion frequencies, adhesion forces, and rupture lengths (Figure 4A, 4B, 4C, and 4D). These data rule out that flagellar or constitutive envelope structures play a major role in swarmer cell hydrophobic adhesion, and strongly suggest that pili are responsible for this property.

Multiadhesive Signatures of Tad Pili. In contrast to nonpiliated cells, WT and Δ*fla* swarmer cells displayed typical multipeak force profiles (Figures 4A [insets] and 5A). Given that these cells are mainly monopiliated under standard conditions (see above), we reasoned that these signatures do not arise from the stretching and desorption of multiple pili. Instead, we argue that, upon contact with the hydrophobic substrate, a single pilus filament (two on rare occasions) engages in hydrophobic interactions involving multiple contact points randomly distributed along the pilus. Pulling the cell away from the substrate therefore leads to the serial rupture of multiple hydrophobic contacts.

Careful inspection of more than a thousand FD curves from 20 different cells revealed three distinct force profiles (Figure 5A and 5B). Rupture peaks, i.e. the last adhesion event before the pilus detaches from the substrate, featured (i) a linear region where force is directly proportional to extension, (ii) a nonlinear region well fitted by the worm-like chain (WLC) model of polymer extension,[32] or (iii) a plateau of constant force with variable length. In addition, we note that, for the three signatures, multiple peaks were observed before the rupture peaks, most likely resulting from the rupture of randomly distributed hydrophobic contacts along the pilus length, as mentioned above.

https://doi.org/10.1021/acs.nanolett.1c00215
Nano Lett. 2021, 21, 3075−3082

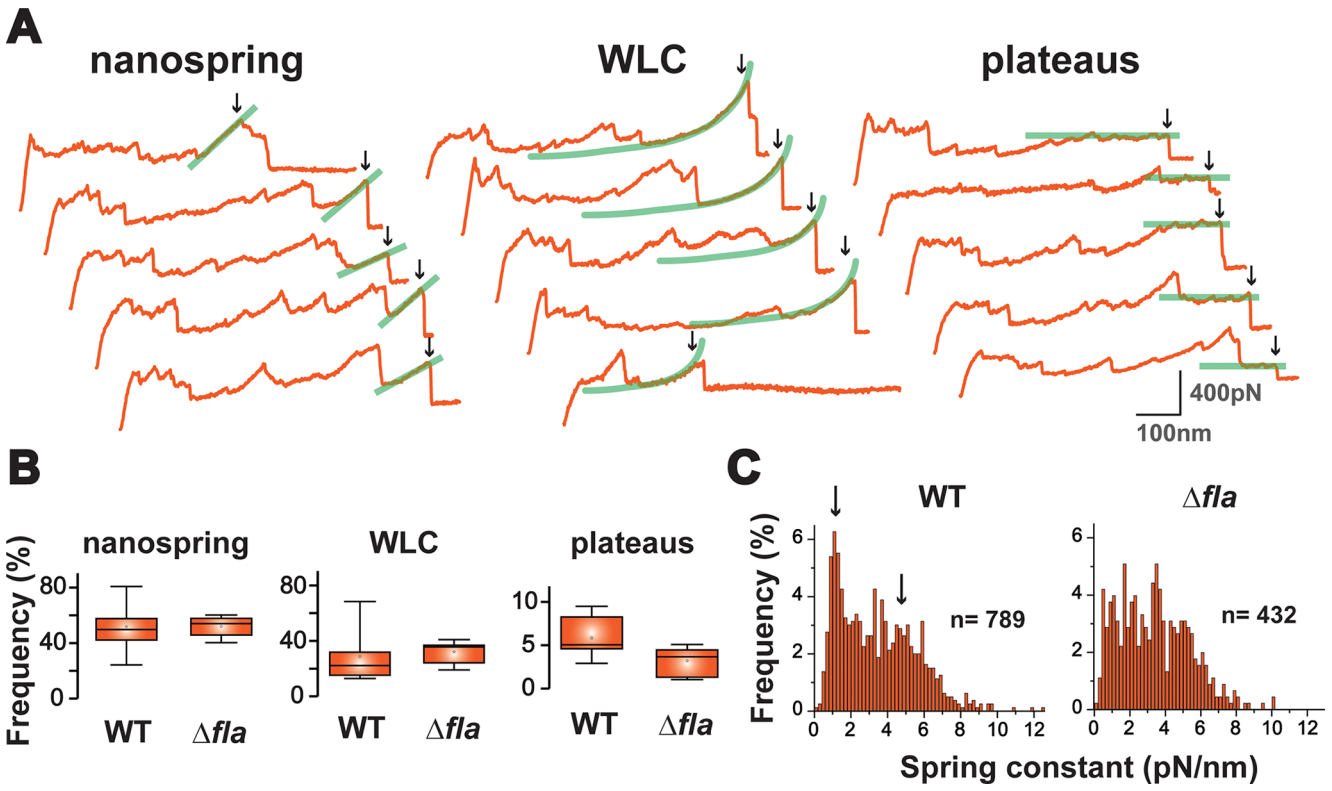

Figure 5. Tad pilus features three distinct adhesion signatures. (A) Five representative retraction force curves obtained on WT cells, in which rupture events are pinpointed with arrows. Green lines emphasize the different adhesive profiles, i.e. nanosprings, worm-like chain extensions, and force plateaus. (B) Boxplots for WT and flagellum-less (Δ*fla*) strains including the mean values (stars), medians (horizontal lines), 1st and 3rd quartiles (box limits), and standard errors (whiskers). Plots were generated from 1,835 adhesion curves (11 independent cells) and 953 adhesion curves (6 independent cells) for the WT and Δ*fla* conditions, respectively. (C) Frequency histograms (%) showing the molecular stiffness distribution for spring-like profiles in the WT and flagellar mutant (Δ*fla*) strains. For the WT, arrows indicate a bimodal distribution. The number of curve segments analyzed on 11 and 6 different cells are indicated.

What is the molecular origin of the above signatures? A large portion of the force curves (53%) featured the linear signature, which is characteristic of a Hookean spring. This shows that the pilus behaves as a nanospring when loaded with tensile stress. Individual Tad pilins do not bind head-to-tail to make a long chain that is rolled up into a helical rod like type I and P pili, in which tensile load acting on the coiled chain unravels it under a constant force (force plateau extension) before the straightened chain is stretched (nonlinear force extension). Instead the hydrophobic N-terminal α-helices of Tad pili are intercalated tightly within the core of the pilus rod giving rise to a more solid core, which most likely explains their nanospring properties. Quantification of the stiffness, i.e. molecular spring constant (k), of the WT nanosprings unveiled a broad, bimodal distribution of values, reaching up to ∼10 pN/nm (Figure 5C). Such a broad distribution may arise from the stretching of filaments with different lengths, as well as from variations in the contact angle between the substratum and the adhering pilus. These results suggest that T4cP are stiffer than T4aP from *P. aeruginosa* (k = ∼2 pN/nm).[9] In the absence of all flagellin genes, signature frequencies were not different compared to the WT strain (Figure 5B). The mutant and WT strains showed rather similar k distributions (Figure 5C), thus further substantiating that Tad pili, and not flagella, exhibit spring-like mechanical responses.

About 30% of the curves from the WT and the flagellar mutant exhibited a WLC signature. The WLC theory describes the extension of a continuously flexible isotropic rod, which is analogous to a relatively stiff, semiflexible polymer, and is generally appropriate to describe protein unfolding.[32] It is unlikely that Tad pilins will unfold because pilins are intercalated within the rod, and unfolding would destabilize the whole fiber. Also, the lengths of WLC peaks were in the 100−200 nm range, which is way larger than expected for pilin unfolding events (45 residues per pilin). We suggest that WLC profiles reflect force-induced extension, and possibly slight conformational changes, in the pilus fiber.

Constant force plateaus were rarely observed (5%), in contrast to *P. aeruginosa* T4aP[9,10] and *E. coli* T1P[33] where they occur frequently. This behavior is generally attributed to the sequential unwinding of the pili. T1P pilins interact with each other in a head-to-tail orientation forming chains that are wound as hoops around a central axis.[34] The sequential unwinding of each hoop gives rise to the constant force plateaus.[33] Given the peculiar structure of T4 cP where the pilins are interlaced within the pilin rod, and the very low occurrence of force plateaus, we believe that these features originate from the sequential rupture of zipper-like interactions involving multiple proximate hydrophobic contacts distributed along the adhering pilus.

DISCUSSION

Substratum docking via extracellular appendages is key in the active flagellum-independent motion of unicellular organisms. The stickiness and mechanical robustness of the Tad pilus are supposed to be crucial in this process, yet this is still poorly

https://doi.org/10.1021/acs.nanolett.1c00215
Nano Lett. 2021, 21, 3075−3082

understood. Our nanoscale images captured the morphology of Tad filaments, illuminating a diameter of 1.5 nm. These pili may thus potentially represent the thinnest pilus-type bacterial appendage. They are markedly slimmer than T1P, conjugative pili, and pili from Gram-positive bacteria, as well as the canonical *P. aeruginosa* T4aP (from 4 to 6 nm).[28] This observation is consistent with the very short size (45 residues) of the Tad pilin subunit, PilA, compared to T4aP PilA (150 residues).

Implementation of SCFS with a fluorescence-based screen enabled the selective probing of living bacteria that assemble pili and provided the first insights into the hydrophobic adhesion and mechanics of Tad pili. One could argue that our method probes multiple pilus filaments decorating the same cell. However, this is unlikely as our images indicate the presence of a single polar pilus in the majority of WT piliated swarmer cells. Additionally, our positive (flagellum mutant) and negative (pilus mutant and nonpiliated WT cells) controls demonstrate that the adhesion profile is mainly due to the pilus and not to other extracellular structures (Figure 4A, 4B, 4C, and 4D). So the observed force profiles can be specifically ascribed to the probing of single pili. Constitutive overproduction of pilus components drives the assembly of multiple pili of similar structure at the same pole (Figure 2A, 2B, 2D and 2E).

Our main finding is that the unipolar Tad pilus exhibits three adhesive behaviors when pulled away from a hydrophobic surface. The most frequently observed pulling curves feature multiple peaks followed by a final rupture peak with a linear slope. This suggests that Tad filaments preferentially bind via hydrophobic interactions distributed over the fiber length, in line with the notion that the pilin subunits are hydrophobic. The last rupture events behave like molecular springs which can sustain high loads (up to 600 pN) without substantial unfolding, thus showing they are mechanically strong. The high rupture forces suggest that the pilus end is very hydrophobic, making multiple hydrophobic contacts that rupture in parallel. We speculate that the high mechanical stability comes from the unusual structure of the Tad pilus, consisting of individual pilins held in place by noncovalent interpilin interactions and presumably tightly arranged in a helical pattern around the central axis of the filament. Pilins are predicted to be composed of two α-helices separated by a hinge that orientates the two helices in slightly different directions. Their hydrophobic N-terminal α-helices are intercalated tightly within the core of the pilus rod giving rise to a more solid structure than other Gram-negative pili. The second type of multipeak force profiles present nonlinear WLC rupture peaks. Given the length of these events and the high stability of Tad pilins, we suggest these profiles reflect the stretching, and perhaps gentle conformational changes, of the pilin subunits, as well as of some components of the pilus portal such as the secretin, the inner membrane core, and the stabilization proteins. Finally, the rarely observed force plateaus would reflect the unzipping of a continuous sequence of hydrophobic contacts between the pilus and the substrate.

The high adhesion frequency (Figure 4B) demonstrates the strong capability of Tad pili to stick to hydrophobic substrates, even at small interaction times. The pilus adhesion is strong (forces around 250 pN, but sometimes up to 600 pN; Figure 4C) compared to the adhesion of *Pseudomonas* T4aP (100–150 pN).[9] This Tight adherence, from where the Tad pilus actually took its name, presumably compensates for the single assembled filament per cell in *Caulobacter* and suggests an alternative strategy to the multiple low-binding fibers that cooperate in the case of T4aP. It is tempting to speculate that the assembly of a unique pilus at one pole of swarmer cells diminishes trans-aggregation of Tad filaments, contributing to a more efficient sedentary switch, from swarmer-to-stalked cells.

Widely distributed in prokaryotes and highly important for cell survival in competitive environments, the Tad pilus is currently gaining much interest, especially at the single filament level. Our results illuminate the remarkable Tad fiber adhesion and mechanics and pave the way for further investigations to identify chemical compounds able to block bacterial adhesion for a medical scope.

■ ASSOCIATED CONTENT

Supporting Information

The Supporting Information is available free of charge at https://pubs.acs.org/doi/10.1021/acs.nanolett.1c00215.

Experimental methods and references (PDF)

■ AUTHOR INFORMATION

Corresponding Authors

Yves F. Dufrêne − *Louvain Institute of Biomolecular Science and Technology, UCLouvain, B-1348 Louvain-la-Neuve, Belgium;* orcid.org/0000-0002-7289-4248; Email: yves.dufrene@uclouvain.be

Johann Mignolet − *Louvain Institute of Biomolecular Science and Technology, UCLouvain, B-1348 Louvain-la-Neuve, Belgium;* orcid.org/0000-0002-3721-4307; Email: johann.mignolet@uclouvain.be

Authors

Albertus Viljoen − *Louvain Institute of Biomolecular Science and Technology, UCLouvain, B-1348 Louvain-la-Neuve, Belgium*

Marion Mathelié-Guinlet − *Louvain Institute of Biomolecular Science and Technology, UCLouvain, B-1348 Louvain-la-Neuve, Belgium;* orcid.org/0000-0001-9023-3470

Felipe Viela − *Louvain Institute of Biomolecular Science and Technology, UCLouvain, B-1348 Louvain-la-Neuve, Belgium*

Claire Valotteau − *Louvain Institute of Biomolecular Science and Technology, UCLouvain, B-1348 Louvain-la-Neuve, Belgium*

Complete contact information is available at: https://pubs.acs.org/10.1021/acs.nanolett.1c00215

Author Contributions

J.M. and Y.D.: Conception and design. J.M.: Acquisition of data. J.M., A.V., F.V., M.M., C.V., and Y.D.: Analysis and interpretation of data. J.M., A.V., F.V., M.M., and Y.D.: Writing of the manuscript.

Notes

The authors declare no competing financial interest.

■ ACKNOWLEDGMENTS

We are grateful to Prof. P. H. Viollier and Dr. Gaël Panis for providing the hyperpiliated mutant and the *pleC-gfp* reporter plasmid. Work at UCLouvain was supported by the Excellence of Science-EOS programme (Grant No. 30550343), the European Research Council (ERC) under the European Union's Horizon 2020 research and innovation programme

(Grant Agreement No. 693630), the FNRS-WELBIO (Grant No. WELBIO-CR-2015A-05), and the National Fund for Scientific Research (FNRS). Y.D. is Research Director at the FNRS.

REFERENCES

(1) Graham, K. J.; Burrows, L. L. More than a feeling: microscopy approaches to understanding surface-sensing mechanisms. *J. Bacteriol.* **2020**, *203*, 1−11.
(2) Craig, L.; Forest, K. T.; Maier, B. Type IV pili: dynamics, biophysics and functional consequences. *Nat. Rev. Microbiol.* **2019**, *17*, 429−440.
(3) Berry, J. L.; Pelicic, V. Exceptionally widespread nanomachines composed of type IV pilins: the prokaryotic Swiss Army knives. *FEMS Microbiol. Rev.* **2015**, *39*, 134−54.
(4) Craig, L.; Pique, M. E.; Tainer, J. A. Type IV pilus structure and bacterial pathogenicity. *Nat. Rev. Microbiol.* **2004**, *2*, 363−78.
(5) Dumenil, G. Type IV pili as a therapeutic target. *Trends Microbiol.* **2019**, *27*, 658−661.
(6) Thomas, W.; Forero, M.; Yakovenko, O.; Nilsson, L.; Vicini, P.; Sokurenko, E.; Vogel, V. Catch-bond model derived from allostery explains force-activated bacterial adhesion. *Biophys. J.* **2006**, *90*, 753−64.
(7) Viela, F.; Mathelie-Guinlet, M.; Viljoen, A.; Dufrene, Y. F. What makes bacterial pathogens so sticky? *Mol. Microbiol.* **2020**, *113*, 683−690.
(8) Biais, N.; Higashi, D. L.; Brujic, J.; So, M.; Sheetz, M. P. Force-dependent polymorphism in type IV pili reveals hidden epitopes. *Proc. Natl. Acad. Sci. U. S. A.* **2010**, *107*, 11358−63.
(9) Beaussart, A.; Baker, A. E.; Kuchma, S. L.; El-Kirat-Chatel, S.; O'Toole, G. A.; Dufrene, Y. F. Nanoscale adhesion forces of *Pseudomonas aeruginosa* type IV Pili. *ACS Nano* **2014**, *8*, 10723−33.
(10) Lu, S.; Giuliani, M.; Harvey, H.; Burrows, L. L.; Wickham, R. A.; Dutcher, J. R. Nanoscale pulling of type IV pili reveals their flexibility and adhesion to surfaces over extended lengths of the pili. *Biophys. J.* **2015**, *108*, 2865−75.
(11) Miller, E.; Garcia, T.; Hultgren, S.; Oberhauser, A. F. The mechanical properties of *E. coli* type 1 pili measured by atomic force microscopy techniques. *Biophys. J.* **2006**, *91*, 3848−56.
(12) Denise, R.; Abby, S. S.; Rocha, E. P. C. Diversification of the type IV filament superfamily into machines for adhesion, protein secretion, DNA uptake, and motility. *PLoS Biol.* **2019**, *17*, No. e3000390.
(13) Mignolet, J.; Panis, G.; Viollier, P. H. More than a Tad: spatiotemporal control of *Caulobacter pili*. *Curr. Opin. Microbiol.* **2018**, *42*, 79−86.
(14) Tomich, M.; Planet, P. J.; Figurski, D. H. The tad locus: postcards from the widespread colonization island. *Nat. Rev. Microbiol.* **2007**, *5*, 363−75.
(15) Giltner, C. L.; Nguyen, Y.; Burrows, L. L. Type IV pilin proteins: versatile molecular modules. *Microbiol. Mol. Biol. Rev.* **2012**, *76*, 740−72.
(16) Del Medico, L.; Cerletti, D.; Schachle, P.; Christen, M.; Christen, B. The type IV pilin PilA couples surface attachment and cell-cycle initiation in *Caulobacter crescentus*. *Proc. Natl. Acad. Sci. U. S. A.* **2020**, *117*, 9546−9553.
(17) Viljoen, A.; Mignolet, J.; Viela, F.; Mathelie-Guinlet, M.; Dufrene, Y. F. How microbes use force to control adhesion. *J. Bacteriol.* **2020**, *202*, 1−10.
(18) Mignolet, J.; Holden, S.; Berge, M.; Panis, G.; Eroglu, E.; Theraulaz, L.; Manley, S.; Viollier, P. H. Functional dichotomy and distinct nanoscale assemblies of a cell cycle-controlled bipolar zinc-finger regulator. *Elife* **2016**, *5*.
(19) Ellison, C. K.; Kan, J.; Dillard, R. S.; Kysela, D. T.; Ducret, A.; Berne, C.; Hampton, C. M.; Ke, Z.; Wright, E. R.; Biais, N.; Dalia, A. B.; Brun, Y. V. Obstruction of pilus retraction stimulates bacterial surface sensing. *Science* **2017**, *358*, 535−538.
(20) Lagenaur, C.; Agabian, N. *Caulobacter crescentus* pili: structure and stage-specific expression. *J. Bacteriol.* **1977**, *131*, 340−6.
(21) Skerker, J. M.; Shapiro, L. Identification and cell cycle control of a novel pilus system in *Caulobacter crescentus*. *EMBO J.* **2000**, *19*, 3223−34.
(22) Smit, J.; Hermodson, M.; Agabian, N. *Caulobacter crescentus* pilin. Purification, chemical characterization, and NH2-terminal amino acid sequence of a structural protein regulated during development. *J. Biol. Chem.* **1981**, *256*, 3092−7.
(23) Kachlany, S. C.; Planet, P. J.; Desalle, R.; Fine, D. H.; Figurski, D. H.; Kaplan, J. B. flp-1, the first representative of a new pilin gene subfamily, is required for non-specific adherence of *Actinobacillus actinomycetemcomitans*. *Mol. Microbiol.* **2001**, *40*, 542−54.
(24) Tripathi, P.; Dupres, V.; Beaussart, A.; Lebeer, S.; Claes, I. J.; Vanderleyden, J.; Dufrene, Y. F. Deciphering the nanometer-scale organization and assembly of *Lactobacillus rhamnosus* GG pili using atomic force microscopy. *Langmuir* **2012**, *28*, 2211−6.
(25) Ellison, C. K.; Rusch, D. B.; Brun, Y. V. Flagellar mutants have reduced pilus synthesis in *Caulobacter crescentus*. *J. Bacteriol.* **2019**, *201*, 1−12.
(26) Borgeaud, S.; Blokesch, M. Overexpression of the tcp gene cluster using the T7 RNA polymerase/promoter system and natural transformation-mediated genetic engineering of *Vibrio cholerae*. *PLoS One* **2013**, *8*, No. e53952.
(27) Meyrand, M.; Guillot, A.; Goin, M.; Furlan, S.; Armalyte, J.; Kulakauskas, S.; Cortes-Perez, N. G.; Thomas, G.; Chat, S.; Pechoux, C.; Dupres, V.; Hols, P.; Dufrene, Y. F.; Trugnan, G.; Chapot-Chartier, M. P. Surface proteome analysis of a natural isolate of *Lactococcus lactis* reveals the presence of pili able to bind human intestinal epithelial cells. *Mol. Cell. Proteomics* **2013**, *12*, 3935−47.
(28) Touhami, A.; Jericho, M. H.; Boyd, J. M.; Beveridge, T. J. Nanoscale characterization and determination of adhesion forces of *Pseudomonas aeruginosa* pili by using atomic force microscopy. *J. Bacteriol.* **2006**, *188*, 370−7.
(29) Rosenberg, M.; Kjelleberg, S. Hydrophobic interactions: Role in bacterial adhesion. *Adv. Microb. Ecol.* **1986**, *9*, 353−393.
(30) Wheeler, R. T.; Shapiro, L. Differential localization of two histidine kinases controlling bacterial cell differentiation. *Mol. Cell* **1999**, *4*, 683−94.
(31) Beaussart, A.; El-Kirat-Chatel, S.; Sullan, R. M.; Alsteens, D.; Herman, P.; Derclaye, S.; Dufrene, Y. F. Quantifying the forces guiding microbial cell adhesion using single-cell force spectroscopy. *Nat. Protoc.* **2014**, *9*, 1049−55.
(32) Bustamante, C.; Marko, J. F.; Siggia, E. D.; Smith, S. Entropic elasticity of lambda-phage DNA. *Science* **1994**, *265*, 1599−600.
(33) Forero, M.; Yakovenko, O.; Sokurenko, E. V.; Thomas, W. E.; Vogel, V. Uncoiling mechanics of *Escherichia coli* type I fimbriae are optimized for catch bonds. *PLoS Biol.* **2006**, *4*, e298.
(34) Habenstein, B.; Loquet, A.; Hwang, S.; Giller, K.; Vasa, S. K.; Becker, S.; Habeck, M.; Lange, A. Hybrid structure of the type 1 pilus of uropathogenic *Escherichia coli*. *Angew. Chem., Int. Ed.* **2015**, *54*, 11691−5.

https://doi.org/10.1021/acs.nanolett.1c00215
Nano Lett. 2021, 21, 3075−3082